Click Here for Full Article

Buoyant melting instabilities beneath extending lithosphere: 1. Numerical models

John W. Hernlund,[1,2] Paul J. Tackley,[1,3] and David J. Stevenson[4]

[1]   Buoyant decompression melting instabilities in regions of partially molten upper mantle have been proposed to be an important process that might account for some characteristics of intraplate volcanism on Earth and other terrestrial planets. The instability is driven by variations in the melting rate within a partially molten layer whenever a relative decrease in density accompanies decompression melting of ascending mantle. Here, the development of buoyant decompression melting instabilities in a plane layer of passively upwelling and partially melting mantle beneath diffusely extending lithosphere is studied using numerical convection models covering a wide range of physical parameters. We find that the occurrence and nature of these instabilities in such a scenario is strongly affected by the rate of extension and melt percolation, as well as depth distribution of solid density variations arising from melt depletion. In some cases, instabilities do not occur during extension, but only develop after extension has slowed or stopped completely. This behavior creates two pulses of magma generation due to passive upwelling accompanying extension followed by the subsequent instability and is favored by a faster rate of extension, higher mantle viscosity, higher rate of melt percolation, and smaller amount of solid residuum depletion-derived buoyancy. Larger degrees of solid density changes accompanying melt depletion can enhance the instability of partially molten mantle during extension but decrease the cumulative volume of generated melt. This kind of behavior modifies the conventional expectation of spatially and temporally correlated volcanism and extension and may lend insight into the observed increase in localized volcanic activity following Miocene Basin and Range extension in the western United States.

Citation: Hernlund, J. W., P. J. Tackley, and D. J. Stevenson (2008), Buoyant melting instabilities beneath extending lithosphere: 1. Numerical models, *J. Geophys. Res.*, *113*, B04405, doi:10.1029/2006JB004862.

1.   Introduction

[2]   If a portion of Earth's upper mantle crosses the solidus during ascent and undergoes decompression melting, in most circumstances its density will decrease. The smaller density is due to the larger molar volume of any retained melt in the matrix as well as changes in composition and/or phase abundance in the residual solid rock. So long as the upward percolation of melt through the solid matrix is not instantaneous, a small fraction of melt will be retained which, along with solid residuum density changes, is available to drive buoyant flow in the partially molten region. Because the buoyancy of partially melted mantle relative to any adjacent unmelted (or less melted) mantle increases as both its upward displacement and velocity increases, a positive feedback can arise that causes internal instability (i.e., runaway convective overturn) of a partially molten region (see Figure 1). This "Rayleigh-Taylor-like" melting instability [*Stevenson*, 1988] may carry important implications for the dynamics of the mantle asthenosphere and the production of melt in Earth's mantle. This process has more recently been termed a "buoyant decompression melting instability" [*Raddick et al.*, 2002], and has been suggested to be a potentially important source of intraplate volcanism on Earth as well as other terrestrial planets [*Tackley and Stevenson*, 1993; *Raddick et al.*, 2002].

[3]   The simplest example of a Rayleigh-Taylor instability is the classical scenario where one fluid is overlain by another fluid of greater density. In this gravitationally unstable arrangement, the smallest perturbation will lead to growing corrugations in the interface between the two fluids as they undergo gravity-driven exchange at a rate controlled by their viscosities and relative buoyancy. An asthenospheric instability of this type was suggested by *Anderson and Sammis* [1970] whenever lower-density partially molten layers in Earth's mantle is overlain by higher density lithosphere. Such mechanisms have been proposed

---

[1]Department of Earth and Space Sciences, University of California, Los Angeles, California, USA.
[2]Now at Department of Earth and Ocean Sciences, University of British Columbia, Vancouver, British Columbia, Canada.
[3]Now at Institute for Geophysics, ETH-Zurich, Zurich, Switzerland.
[4]Division of Geological and Planetary Sciences, California Institute of Technology, Pasadena, California, USA.
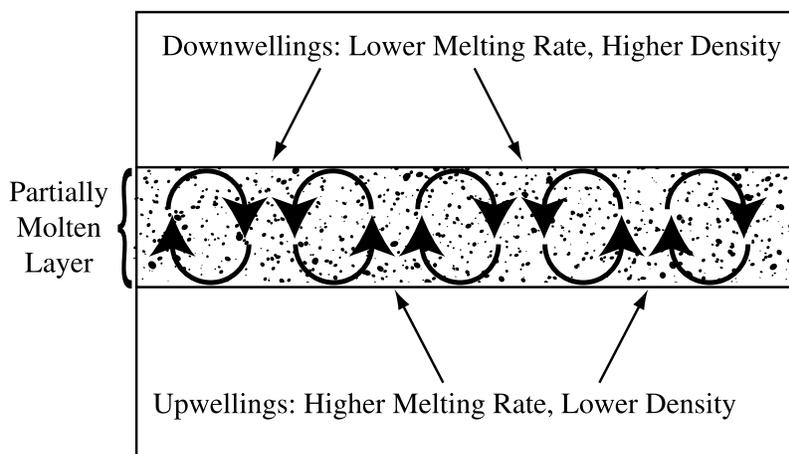
Figure 1. Illustration showing the cause of a runaway instability within a partially molten layer. Upward motion is associated with increased rates of melting relative to downward motion. The density is reduced as a consequence of melting so that upwellings become more buoyant, move upward at a faster rate, and generate more melt. This positive feedback can lead to convective overturn of the layer and might potentially generate significant amounts of melt.

to account for the inferred length scales of buoyant melt diapirism beneath mid-ocean ridges [*Whitehead et al.*, 1984; *Crane*, 1985] and arc volcanoes [*Lingenfelter and Schubert*, 1974]. Complex interactions between Rayleigh-Taylor two-phase instabilities under the additional influence of melt percolation have also been analyzed by *Ricard et al.* [2001]. However, the buoyant decompression melting instability differs from the classical scenario in several ways. This is because it does not directly involve the mantle lithosphere (which may be too viscous to flow in response to the available forces) and because the buoyancy which drives the flow develops as a direct consequence of variations in the rate of melting within the layer rather than unstable displacement of the entire layer (although external influences may also play an important role). Additional complications include the fact that the generation of buoyancy within a partially molten layer may be asymmetric, in that only upwellings undergo active melting while adjacent downwellings remain unchanged if they are initially unmelted or contain very little or no melt [*Tackley and Stevenson*, 1993]. The primary similarities between the decompression melting instability and the classical Rayleigh-Taylor scenario are its inherently limited duration and apparent unconditional instability [*Tackley and Stevenson*, 1993; *Raddick et al.*, 2002].

[4] There also exist distinctions between the buoyant decompression melting instability and the enhanced instability caused by interaction between thermal convection and partial melting. Although important interactions of this kind have been studied in the context of mid-ocean ridges [*Scott and Stevenson*, 1989; *Buck and Su*, 1993], and mantle plumes [*Ribe and Christensen*, 1999], the buoyant decompression melting instability is different because it is derived from an inherent internal instability of a "two-phase" (i.e., melt + solid) region. This instability need not be an enhancement of larger-scale convection, but rather is a process which could develop independently in the absence of significant lateral temperature variations in the mantle.

However, the existence of any sort of background thermal or chemical heterogeneity would likely serve as a nucleation point for instability, causing activity associated with this phenomenon to be preferentially correlated with changes in deep-rooted lithospheric structure [*Raddick et al.*, 2002].

[5] The basic requirements for the occurrence of a buoyant melting instability are that a layer of mantle be brought to the solidus temperature for a "sufficient" period of time, adiabatic upwelling leads to further melting, and such melting results in a cumulative decrease in density in upwelling regions relative to downwelling regions. This is also subject to the more fundamental requirement that the layer of mantle not be too depleted that it cannot produce more melt. There are numerous processes by which a portion of mantle may be brought to the solidus temperature, such as upwelling of deep mantle that has risen under its own buoyancy (e.g., a mantle plume head or its wake) or under the influence of tectonic activity (e.g., beneath extending continental lithosphere or mid-ocean ridges). A region of mantle brought to the solidus does not immediately cool, but may remain at or near this temperature until thermal conduction or some other process modifies its state. The timescale for conductive cooling of a partially melted region several tens of km in dimension is typically on the order of several million years. So long as the instability manifests itself on shorter timescales, a partially melted region may be susceptible to the occurrence of buoyant melting instabilities.

[6] Basaltic melt extracted from a typical "dry" upper mantle peridotite can be up to about 15% less dense than the source rock, although this value varies widely with pressure and composition [e.g., *Stolper and Walker*, 1980]. Because it is a partial melt, its actual contribution to bulk density variations is proportional to the volume fraction of retained melt ϕ, which is expected to be small (of order 1%) in the upper mantle. The total contribution of melt to density variations is therefore on the order of 0.15%. Density changes in the solid residuum following melt extraction

are an inevitable consequence of incongruent fractional melting, and is attributed to two effects: (1) a change in chemistry of individual mineral phases comprising the rock due to preferential partitioning of some of its dissolved components into the melt and (2) a change in the volumetric abundance of different crystalline phases, each of which has a different density. The relative importance of these two mechanisms is sensitive to solid-solid phase changes, such as the spinel-garnet transition occurring at ∼70–80 km depth in Earth's mantle, because garnet is a dense phase and is preferentially consumed by melting. Density changes also occur because the Fe/Mg ratio of depleted rock is often smaller than unmelted rock. The calculations of *Oxburgh and Parmentier* [1977] yielded a density reduction of about 1.5% for 15% fractional melting of peridotite in the garnet stability field, and about half this amount in the spinel stability field, similar to estimates reported by *Jordan* [1979]. Recent estimates by *Schutt and Lesher* [2006] using improved experimental data found a 1.2% density reduction in the garnet stability field after 20% melt extraction and much smaller density changes for melt extraction in the spinel stability field. Thus the degree to which melt extraction in the spinel stability field affects solid density may be significantly smaller than previously thought. Thermal buoyancy may also become important in a partially melted layer if temperature variations are not strongly buffered by latent heat effects associated with melting. Temperature changes density by $\alpha \Delta T$, where α is the thermal expansivity and ΔT is the magnitude of horizontal temperature variations. Assuming a typical value of $\alpha = 3 \times 10^{-5}$ K^{-1} and $\Delta T = 50$ K yields a 0.15% density change. Thus in summary, a temperature increase of 50 K yields the same density variation as 1% increase in melt fraction, or about 1.5% melt extracted from garnet peridotite. However, this ratio is also generally variable because depletion also affects the thermal expansivity of mantle rocks [*Schutt and Lesher*, 2006].

[7] The full physics of the buoyant decompression melting instability is complex because it involves up to three sources of buoyancy for the bulk circulation, each of which is governed by different transport processes. Temperature variations are subject to thermal diffusion, and additionally can be affected by the absorption (or release) of latent heat whenever melting (or freezing) occurs. Solid composition and phase variations arise from partial melting and segregation, and unlike temperature variations do not diffuse away at a significant rate over the relevant spatiotemporal scales. Partial melt is more complicated, because it may undergo gravity-driven percolation through the pore spaces it occupies in the solid matrix, which can accelerate its removal up and out of regions where it is produced. Although percolation is not a strictly diffusive process, it may still act as a dampening agent in this kind of instability by removing a source of buoyancy and weakening the strength of any unstable circulation driven by lateral variations in partial melt fractions. A straightforward analysis of the effects of percolation is also complicated by the fact that the rate of melt migration is itself dependent upon the amount of melt present in the rock as well as a variety of potentially complex microstructural processes.

[8] *Tackley and Stevenson* [1993] first studied this kind of instability using convection models including the effects of melt buoyancy, a simple univariant melting model, and percolation of the melt according to Darcy's law. They ignored the effects of thermal and melt depletion buoyancy in order to isolate the role of melt retention buoyancy and percolation. Beginning with an initial condition where the mantle finds itself at the solidus temperature over a layer of thickness D, the duration and volume of melt generated by the instability were found to depend strongly (and nonlinearly) upon the rate of melt percolation. When scaled to geologically relevant ranges of parameters, characteristic velocities of order 3 cm a^{-1} and durations of order several million years were obtained from their numerical results. The spacing between upwellings was found to be about 2–3 X the thickness of the partially molten layer, which defines a characteristic length scale for the occurrence of volcanic activity which might arise as a consequence of these kinds of instabilities.

[9] *Jha et al.* [1994] considered the occurrence of this kind of instability beneath the axis of mid-ocean ridges using melt retention and depletion buoyancy, following earlier work that only considered melt depletion buoyancy [*Parmentier and Morgan*, 1990]. Such instabilities can generate three-dimensional structure in an otherwise two-dimensional ridge setting. These studies demonstrated that the instabilities only occur beneath a ridge for slower plate spreading rates, perhaps explaining why slow spreading ridges exhibit more along axis variability than fast spreading ridges [*Parmentier and Morgan*, 1990], though not at all length scales [*Barnouin-Jha et al.*, 1997] unless the influence of variable viscosity is taken into account [*Choblet and Parmentier*, 2001]. The influence of melt buoyancy was found to be strongly controlled by the grain size, which modulates the rate of melt percolation and hence the retained fraction of melt in the mantle. The study of *Barnouin-Jha et al.* [1997] also considered buoyancy arising from temperature variations beneath a ridge, in addition to melt retention and solid depletion effects, and found a variety of behavior for instabilities occurring beneath and away from the ridge axis, and suggested that the occurrence of these different behaviors must be controlled by some type of effective "Rayleigh number."

[10] *Schmeling* [2000] considered the rate of propagation of this type of instability across an initially uniform partially molten asthenospheric layer. An experimentally constrained power law rheology was adopted, and partially molten regions were assigned a "wet" rheology. The physics of the two-phase (melt + solid) flow was treated using a "compaction Boussinesq approximation" that was designed to account for the effects of matrix stresses on melt percolation while still maintaining some simple features of the standard Boussinesq approximation. The rate of propagation of the instability was found to be on the order of several centimeters per year, and was compared to the motion of hot spots. Circulation was largely confined to the partially molten layer, most likely because it was assigned a lower viscosity than other portions of the model domain.

[11] *Raddick et al.* [2002] completed the most recent systematic study of the instability, treating the effects of thermal, solid depletion, and melt buoyancy along with viscosity variations induced by melting in a plane layer of asthenosphere. Percolation was not explicitly modeled,
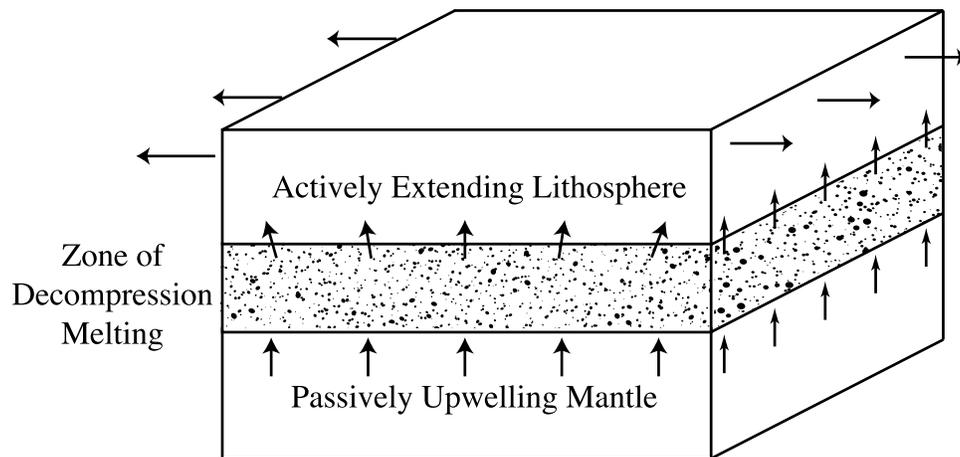
Figure 2. Schematic illustration of passive decompression melting in a plane layer of mantle accompanying distributed lithospheric extension.

rather a threshold criterion was used instead where the melt was considered to escape instantly after reaching a critical value. They found that the duration and amount of melt generated by this kind of instability can be strongly affected by preexisting melt depletion buoyancy. Another signature characteristic of this instability was found to be a duration that is inversely proportional to the volume of melt produced, a feature that is apparently related to solid depletion buoyancy effects. Additionally, the spacing between upwellings was found to be slightly sensitive to the relative importance of thermal and compositional buoyancy, with spacing becoming smaller with increasing solid depletion-derived buoyancy.

[12] The goal of the present study is to consider the occurrence of these kinds of instabilities beneath diffusely extending lithosphere, an important and common geological process on Earth in which partial melting of the mantle is commonly attributed to simple passive upwelling of the mantle. Numerical models are used to study the development of buoyant decompression melting instabilities under a variety of extension rates, mantle viscosities, rates of melt percolation, and effects of solid depletion-related buoyancy. We then discuss a possible application of the wide variety of observed behaviors to the complex spatial and temporal relationships between volcanism and extension in the western U.S. Basin and Range province. The companion paper by *Hernlund et al.* [2008] (hereafter referred to as HST) employs a linear analysis in order to interpret these numerical results and to obtain a better understanding of the basic processes leading to the onset of buoyant decompression melting instabilities. Further applications of this theory to melting instabilities beneath mid-ocean ridges are also discussed in HST.

[13] The setting for the models performed in this study is the simplest possible scenario for bringing a layer of mantle above the solidus temperature without introducing spurious perturbations or external influences: passive decompression melting of a plane layer of mantle as it upwells in response to regional (diffuse) lithospheric extension (Figure 2). In contrast to the study of these instabilities beneath mid-ocean

ridges [*Parmentier and Morgan*, 1990; *Jha et al.*, 1994; *Barnouin-Jha et al.*, 1997], the basic setting for the instability is essentially one-dimensional rather than two-dimensional, which allows us to isolate different behaviors of the instability from confounding influences and other factors that may arise in more complex settings. There are additional motivations for studying buoyant decompression melting instabilities beneath diffusely extending lithosphere. First, the generation of mantle melt in regions undergoing diffuse lithospheric extension represents an important source of volcanism away from plate boundaries. Any instability of this kind occurring in such a setting will inevitably have an impact upon the volumes, timing, and length scales of volcanism observed at the surface which cannot be accounted for by simpler one-dimensional models [e.g., *McKenzie and Bickle*, 1988]. Second, the occurrence of this kind of instability beneath the Basin and Range province of the western United States has previously been proposed on the basis of geological and geophysical observations [*Humphreys and Dueker*, 1994a, 1994b], and the basic setting for the model studied here is similar to conditions that are expected to have accompanied the late Cenozoic history of this region.

[14] An important feature of this study is the incorporation of a self-consistent treatment of melt percolation, and it is again found that the rate of this process strongly modulates the dynamics of this kind of instability. It will also be shown that for certain ranges of mantle viscosity, extension and percolation rates, buoyant decompression melting instabilities are suppressed during extension and only begin to develop after extension has slowed or stopped. This behavior is found to be sensitive to both the strength and depth distribution of melt depletion buoyancy. The possibility for an increased rate of localized volcanism following the cessation of extension is predicted to be a distinctive diagnostic characteristic of these kinds of instabilities that may be difficult to produce by any other mechanism. An increase in localized volcanism following extension has been reported in several late Cenozoic volcanic fields in the Basin and Range province [*Gans and Bohrson*, 1998; *Stockli et al.*, 2002], and these kinds of instabilities might

therefore be an important dynamical process that has contributed to the complex geologic history of this region.

2. Mathematical Model

[15] Numerous models have emerged to describe partial melting and two-phase (melt and solid) flow in the mantle [e.g., *McKenzie*, 1984; *Scott and Stevenson*, 1989; *Spiegelman*, 1993; *Schmeling*, 2000; *Bercovici et al.*, 2001]. The situation can either be described by constructing momentum equations governing the melt and solid individually, or alternatively by taking both an average of these equations to obtain a mixture momentum equation and a weighted difference of the two momentum equations to yield an "action-reaction" equation for the separation of fluid and solid. Here, the latter strategy is adopted because it allows for a simple implementation in the numerical routines to be used in this study. The model described here is similar to the one used by *Tackley and Stevenson* [1993], with the inclusion of solid depletion similar to that of *Raddick et al.* [2002]. Although the model we adopt is admittedly simple, it will become clear that it produces a variety of interesting behavior that needs to be thoroughly understood before implementing more complex models.

2.1. Momentum Equations

[16] The kinematics of the melt and solid mixture can be described by assigning to the solid an average matrix velocity $\mathbf{v}_s$, and to the melt an average velocity through the pore spaces $\mathbf{v}_m$. The flow separation is defined as the difference between these two velocities $\mathbf{v}_m - \mathbf{v}_s$, and the bulk (or average/barycentric) velocity of melt and solid is $\mathbf{v} = \phi\mathbf{v}_m + (1 - \phi)\mathbf{v}_s$, where ϕ is the volume fraction of melt. The simplest model for flow separation is percolation driven by the lithostatic pressure gradient according to Darcy's law:

$$u\hat{z} = \phi(\mathbf{v}_m - \mathbf{v}_s) = \frac{k(\phi)(\rho_s - \rho_m)g}{\mu_m}\hat{z}, \qquad (1)$$

where u is the "Darcy velocity" (volume flux of melt through the solid matrix), $\hat{z}$ is an upward directed unit vector, ρ_s is the density of the solid, ρ_m is the melt density, g is the acceleration of gravity, and μ_m is the melt viscosity. For small melt fractions and laminar percolation through quasi-cylindrical pore spaces, the Darcy permeability $k(\phi)$ is approximately $k = k_0\phi^2$, where k_0 is a constant that depends on the shape and size of solid grains [e.g., *Turcotte and Schubert*, 2002, chapter 9]. We note, however, that the particular form of the permeability relation appropriate for Earth's mantle is not well constrained. Equation (1) is an "action-reaction" equation representing the difference in momentum between melt and solid. It assumes that for the length scales of interest in this study, the vertical (lithostatic) pressure gradient is much larger (of order several GPa) than any lateral dynamic pressure gradients arising from mantle flow (of order of several megapascals), and thus melt separation only occurs in the direction of gravity. A posteriori comparison of dynamical pressure gradients from the numerical models reveals that the dynamic pressure gradient is typically at least 2 orders of magnitude smaller than the lithostatic pressure gradient for the present scenario.

[17] The momentum equation for the mixture is written in terms of the bulk velocity, which is taken to be incompressible for simplicity,

$$\nabla \cdot \mathbf{v} = 0. \qquad (2)$$

Assuming the Boussinesq and infinite Prandtl number approximations, the bulk force balance is given by

$$2\nabla \cdot (\mu\nabla\mathbf{v}) + \nabla \times (\mu\nabla \times \mathbf{v}) - \nabla P + \rho\mathbf{g} = 0, \qquad (3)$$

where ∇ is the gradient vector, μ is the viscosity of the mixture, and P is the pressure. Equations (1) and (3) implicitly assume that (1) pressure differences between fluid and solid arising from surface tension effects are negligible, (2) ϕ is small (i.e., of order 1%), (3) μ_m is small in comparison to the solid viscosity μ_s, and (4) matrix compaction due to melt removal occurs instantaneously and without resistance. For the bulk density, ρ, a linearized equation of state is used to measure the response to variations in temperature T, melt fraction ϕ, and degree of solid depletion ζ (defined below), after which the mixture momentum equation becomes

$$2\nabla \cdot (\mu\nabla\mathbf{v}) + \nabla \times (\mu\nabla \times \mathbf{v}) - \nabla p$$
$$= g\hat{z}\left(\frac{\partial\rho}{\partial T}T + \frac{\partial\rho}{\partial\phi}\phi + \frac{\partial\rho}{\partial\zeta}\zeta\right), \qquad (4)$$

where p is the nonhydrostatic pressure. The derivatives $\partial\rho/\partial T$, $\partial\rho/\partial\phi$, and $\partial\rho/\partial\zeta$ are taken to be constant parameters in this study.

2.2. Transport Equations

[18] The conservation of melt is given by [e.g., *McKenzie*, 1984]

$$\frac{\partial\phi}{\partial t} + \nabla \cdot (\mathbf{v}_m\phi) = \frac{\rho_s}{\rho_m}\dot{m}, \qquad (5)$$

or alternatively in terms of the bulk and Darcy velocities,

$$\frac{\partial\phi}{\partial t} + \mathbf{v} \cdot \nabla\phi = -\frac{\partial[u(1 - \phi)]}{\partial z} + \frac{\rho_s}{\rho_m}\dot{m}, \qquad (6)$$

where $\dot{m}$ is melt production rate. For the conservation of energy,

$$\frac{\partial T}{\partial t} + \mathbf{v} \cdot \nabla T = \kappa\nabla^2 T - \frac{L}{c_p}\dot{m}, \qquad (7)$$

where κ is the thermal diffusivity, L is the latent heat of melting, and c_p is the specific heat. In writing equation (7), it is assumed that differences in κ, c_p, etc., between melt and solid are negligible, and that temperature is advected with the bulk velocity. The solid depletion, ζ, is defined as the cumulative volume fraction of melt extracted from the solid, and because it must move with the solid velocity, it is governed by

$$\frac{\partial\zeta}{\partial t} + \nabla \cdot (\mathbf{v}_s\zeta) = \frac{\rho_s}{\rho_m}\dot{m}, \qquad (8)$$
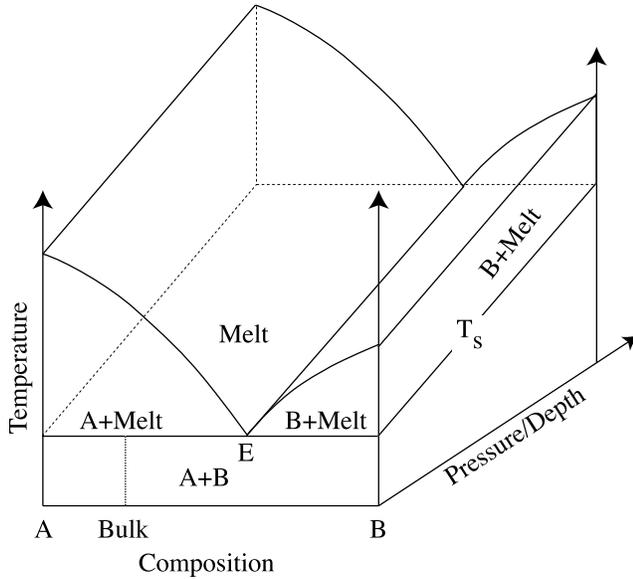
Figure 3. Illustration of the simple eutectic melting model assumed in this study. Melting is considered to take place between two solid phases, A and B, with a "bulk" composition lying between the eutectic E and phase A. Phase B is considered to be more dense than phase A; thus preferential consumption of B by the eutectic melt results in a bulk density decrease in the residual solid.

or in terms of the bulk and Darcy velocities,

$$\frac{\partial \zeta}{\partial t} + \mathbf{v} \cdot \boldsymbol{\nabla} \zeta = \frac{\partial(u\zeta)}{\partial z} + \frac{\rho_s}{\rho_m} \dot{m}. \tag{9}$$

The meaning of ζ can be understood by noting that in the absence of percolation $u \rightarrow 0$, and the conservation equations for melt (equation (5)) and depletion (equation (8)) are exactly the same.

2.3. Melting Model

[19] In this study, density changes in the residual solid are considered to arise primarily as a consequence of the preferential consumption of distinct phases during melting [*Schutt and Lesher*, 2006]. Hence a simple eutectic melting model is adopted, with melt being generated by the reaction between two immiscible solid phases A and B. The bulk composition of undepleted material (i.e., $\zeta = 0$) is taken to lie between pure A and the eutectic composition E (Figure 3) such that melting preferentially consumes phase B. Nonzero degrees of depletion (i.e., $\zeta_0 > 0$) are therefore associated with a higher relative abundance of phase A. Phase B is a generic proxy for a dense solid phase (e.g., garnet), whose preferential consumption by eutectic melting causes the bulk density of the solid to decrease (i.e., $\rho_A < \rho_B$) as a consequence of its decreased volume abundance following melt extraction. For simplicity, the total fraction of melt extracted in the model is considered to be less than the fraction for which B would be entirely consumed (i.e., B_{out}), and therefore the temperature does not rise above the eutectic, nor does the composition of the melt depart from

the eutectic composition E. The eutectic temperature T_s is assumed to be linear in depth h,

$$T_s = T_{s0} + \frac{dT_s}{dh} h, \tag{10}$$

where T_{s0} is the eutectic at the surface ($h = 0$) and dT_s/dh is the rate of change with depth. Because the bulk flow is incompressible in the models considered here, the eutectic slope appearing in equation (10) is defined relative to the potential, rather than absolute, temperature scale. Under the above assumptions, the exact details of the binary eutectic system need not be specified, since the effects of melting upon solid density, melt depletion, and temperature are already specified by the linearized equation of state and latent heat. More realistic melting models in the context of this instability might be worth considering in the future, however, this is beyond the scope of the present study.

[20] Melting can also be described in the context of adiabatic upwelling, where the rate at which mass is converted from solid to liquid, $\dot{m}$, is proportional to the upwelling velocity. At the eutectic temperature, upwelling produces a rate of melting given by

$$\dot{m} = \frac{\rho_m}{\rho_s} F(\hat{z} \cdot \mathbf{v}), \tag{11}$$

where F is the volume fraction of melt produced per unit distance of adiabatic upwelling. Given the above assumptions, the adiabatic melt productivity is related to latent heat by combining equation (11) with equation (7) to give

$$\frac{dT_s}{dh} = \frac{LF}{c_p}. \tag{12}$$

Although F is in reality a complicated function of pressure and composition [e.g., *Asimow et al.*, 1997], it is treated as a constant here for simplicity. It should be noted that our goal in this study is not to reproduce the precise details of mantle melting, but rather to formulate and understand its effects in as simple a way as possible and lay the groundwork for future studies of the instability.
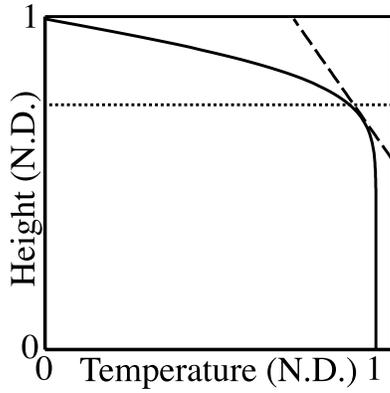
2.4. Nondimensionalization

[21] It is useful to nondimensionalize the governing equations and all quantities relative to a depth scale D, a thermal diffusion time scale D^2/κ, a temperature scale ΔT, a reference viscosity μ_0 and density ρ_0. Indicating nondimensionalized quantities with a prime, the equations of motion become

$$\boldsymbol{\nabla}' \cdot \mathbf{v}' = 0, \tag{13}$$

$$2\boldsymbol{\nabla}' \cdot (\mu'\boldsymbol{\nabla}'\mathbf{v}') + \boldsymbol{\nabla}' \times (\mu'\boldsymbol{\nabla}' \times \mathbf{v}') - \boldsymbol{\nabla}'p'$$
$$= -\hat{z}(Ra T' + Rm\phi + Rd\zeta), \tag{14}$$

$$u'\hat{z} = \phi(\mathbf{v}'_m - \mathbf{v}'_s) = \frac{Rm}{Mr}\phi^2\hat{z}, \tag{15}$$

Figure 4. Initial conditions for temperature (solid line) and the position of the eutectic (dashed line) used in the numerical models. For the choice of parameters used here, the initial temperature is given by erf(depth/0.21). The depth of the spinel-garnet transition used in the "mixed phase" cases (see section 3 for details) is indicated by a dotted line.

$$\frac{\partial T'}{\partial t'} + \mathbf{v}' \cdot \boldsymbol{\nabla}'T' = \nabla'^2 T' - L'\dot{m}', \tag{16}$$

$$\frac{\partial \phi}{\partial t'} + \mathbf{v}' \cdot \boldsymbol{\nabla}'\phi = -\frac{\partial u}{\partial z'} + \dot{m}', \tag{17}$$

$$\frac{\partial \zeta}{\partial t'} + \mathbf{v}' \cdot \boldsymbol{\nabla}'\zeta = \frac{\partial (u\zeta)}{\partial z'} + \dot{m}', \tag{18}$$

where

$$Ra = \frac{\rho_0 g\alpha \Delta T D^3}{\kappa \mu_0}, \tag{19}$$

$$Rm = -\frac{gD^3}{\kappa \mu_0}\frac{\partial \rho}{\partial \phi}, \tag{20}$$

$$Rd = -\frac{gD^3}{\kappa \mu_0}\frac{\partial \rho}{\partial \zeta}, \tag{21}$$

$$Mr = \frac{\mu_m D^2}{\mu_0 k_0}. \tag{22}$$

Ra, Rm, and Rd are the respective "Rayleigh numbers" for temperature, melt, and solid depletion derived buoyancy. The quantity Mr is called a "melt retention" number, since it is inversely proportional to the rate of melt percolation. In the following, the primes on nondimensionalized quantities will be dropped for brevity, and unless stated otherwise variables are nondimensional.

2.5. Numerical Model

[22] Numerical models are performed using the code STAG3D [*Tackley*, 1996]. The governing equations (13)–

(18)) are solved using a finite volume technique in a two-dimensional Cartesian domain of aspect ratio two. A grid density of 32 in the vertical and 64 in the horizontal direction is used for most calculations, and cases run at double this grid density have also been performed to ensure that the resolution is sufficient. The cases are run in two dimensions with the horizontal axis coinciding with the direction of extension, which allows us to explore a large parameter space at relatively small computational expense.

[23] A Newtonian temperature-dependent viscosity is adopted which follows a simple Arrhenius relationship of the form

$$\mu = \exp\left[E_a\left(\frac{1}{T + T_{surf}} - \frac{1}{1 + T_{surf}}\right)\right], \tag{23}$$

where E_a is the nondimensional activation energy (i.e., the dimensional value in kJ mol^{-1} normalized by the gas constant R and ΔT) and T_{surf} is the nondimensional temperature of the surface (i.e., 273 K normalized by ΔT). This rheology gives a strong temperature dependence of the viscosity so that a highly viscous "lithosphere" arises naturally as a consequence of its cooler temperatures, and causes the circulation due to buoyant convection to be confined to the partially molten zone and underlying mantle. The nondimensional viscosity is equal to unity in the underlying mantle, where the temperature is $T = 1$, and is truncated at a maximum value of $\mu = 10^3$, which is more than sufficient to suppress convective motions in the overlying lithosphere.

[24] The initial condition is a geotherm described by a subeutectic error function profile, but which is taken to be very close to the eutectic temperature so that only a small amount of extension is required to induce a partially molten layer of material (Figure 4). In order to isolate the effects of passive upwelling upon the solid depletion profile, initially $\zeta = 0$ everywhere. Random perturbations of 1% are added to the temperature, which are transformed into perturbations in melt and depletion after the temperature exceeds the eutectic. Extension is imposed as a kinematic boundary condition by setting the velocities at the edges of the model domain to match a pure shear flow pattern of the form

$$\mathbf{v} = v_x\hat{x} + v_z\hat{z} = \dot{\varepsilon}[(x - 1)\hat{x} + (1 - z)\hat{z}], \tag{24}$$

where $\hat{x}$ is the unit vector directed along the coordinate x, v_x is the horizontal velocity, v_z is the upward velocity, $\dot{\varepsilon}$ is the strain rate, and $x = 1$ is the x coordinate of the middle of the domain. The pattern of flow that develops in the absence of internal buoyancy forces is plotted in Figure 5. This type of boundary condition assumes that extension is uniformly distributed with depth, which is the simplest possible arrangement and removes the possibility for any potentially complicating effects of background lateral shear flow in the asthenosphere.

[25] The temperature at the top of the domain is set to $T = 0$, while the temperature and depletion are set to $T = 1$ and $\zeta = 0$ at the bottom of the model domain to ensure that fertile material of uniform temperature is advected into the model from below. The run durations are shorter than the time required to develop a lower thermal boundary layer, so that
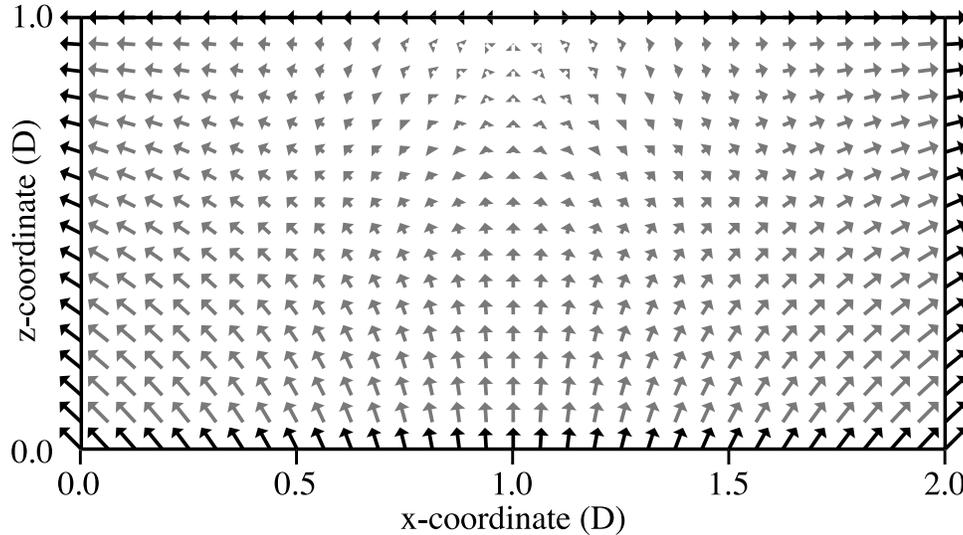
Figure 5. Boundary conditions for the x and z components of velocity (black arrows) and the pattern of pure shear that develops inside the domain in the absence of buoyancy forces (grey arrows). In the numerical models, the internal velocity field (grey arrows) is obtained in accordance with the mathematical model described in the text. The x and z coordinates are measured in units of the domain depth D.

no boundary layer or associated instabilities in the form of upwelling plumes from below occur in the time span of interest. Models with an effective dimensional depth of 670 km have also been performed for a variety of cases to ensure that the side and lower boundary conditions have no significant effect on the results reported here.

[26] The imposed extensional strain rate is taken to be time-dependent ($\dot{\varepsilon} = \dot{\varepsilon}(t)$), and after a prescribed amount of time it tends to zero according to

$$\dot{\varepsilon} = \frac{\dot{\varepsilon}_0}{2}\left(1 - \tanh\left(\frac{5(t - t_s)}{t_s}\right)\right), \qquad (25)$$

where $\dot{\varepsilon}_0$ is a reference strain rate and t_s is a stopping time which is set to produce a given amount of cumulative stretch β according to $t_s = \dot{\varepsilon}_0^{-1} \ln \beta$ (e.g., $\beta = 2$ when the surface is expanded by a factor of 2). The factor of 5 appearing in the argument of the hyperbolic tangent is arbitrarily chosen so that it produces a gradual and smooth transition to a zero rate of extension.

[27] Melt production is treated by a simple energy balance that converts excess temperature into melt fraction via the latent heat in order to satisfy the condition that the temperature remains capped by the eutectic. Freezing is straightforwardly accounted for in this procedure. Because $\phi \to 0$ in the "lithosphere" above the partially molten layer, $u \to 0$ and the melt fraction in the topmost cell of a partially molten column exhibits runaway growth. A threshold criterion for melt "eruption" was used by *Raddick et al.* [2002], where melt was considered to erupt after attaining a critical fraction ϕ_c, thus avoiding this kind of runaway accumulation of melt. However, it will be important in this study to allow the equations to directly govern the melt fraction. Thus we adopt a new kind of filter that removes the excess melt accumulating at the top of a partially molten layer, and mimics the transition to rapid melt transport

through dikes or cracks in the lithosphere. The filter is very simple, and is applied by first finding the uppermost cell in the model domain containing partial melt within every vertical column. A fraction of melt in this uppermost cell in excess of the fraction in the underlying cell is then removed and added to a total cumulative amount of melt "erupted" from the mantle. We note, however, that in reality only a fraction of this "erupted" melt might reach the surface and it therefore represents an upper bound upon any actual expected volcanic eruption rate.

3. Results

[28] Several thousand cases have been investigated, and the results of these runs reveal a variety of interesting behaviors. The parameter values used in the suite of calculations are listed in Table 1. The most uncertain physical parameters are the reference viscosity of the bulk mixture μ_0, the reference Darcy permeability k_0, and the melt viscosity μ_m, which are accordingly varied within a reasonable range of values. The reference strain rate $\dot{\varepsilon}_0$ is also varied (between 1×10^{-15} sec^{-1} and 10^{-14} sec^{-1}) in order to explore the effects of different extension rates upon the characteristics of the instability. The dimensional duration of extension resulting from these extension rates ranges between roughly 2 and 20 Ma for a stretch factor of $\beta = 2$. The contribution of solid depletion to density variations is considered in three distinct scenarios: (1) one in which $\partial \ln\rho/\partial\zeta = 0\%$ throughout the entire model domain (hereafter termed the "spinel stability case"), (2) one in which $\partial \ln\rho/\partial\zeta = 6\%$ throughout the entire model domain (hereafter termed the "garnet stability case"), and (3) one in which a spinel-garnet transition is included with $\partial \ln\rho/\partial\zeta = 6\%$ at depths greater than 80 km and $\partial \ln\rho/\partial\zeta = 0\%$ at shallower depths (hereafter termed the "mixed phase case"). Although this is admittedly oversimplified, it will serve to

Table 1. Parameter Values Considered in This Study

Quantity	Dimensional Values
ρ_0	3300 kg m^{-3}
g	10 m s^{-2}
$\partial\rho/\partial\phi$	-500 kg m^{-3}
$\partial\rho/\partial\zeta$	$0-200$ kg m^{-3}
β	2
$\dot{\varepsilon}_0$	$10^{-15}-10^{-14}$ s^{-1}
α	3×10^{-5} K^{-1}
ΔT	1500 K
μ_0	$10^{19}-10^{21}$ Pa s
κ	10^{-6} m^2 s^{-1}
D	300 km
E_a	500 kJ mol^{-1}
T_{s0}	1400 K
dT_s/dh	3.5 K km^{-1}
F	5×10^{-3} km^{-1}
k_o/μ_m	$10^{10}-10^{12}$ Pa s m^{-12}

illustrate that the behavior of the instabilities under the influence of solid depletion buoyancy depends not only upon the degree of density changes, but also upon the location of density changes within the partially molten layer. Because the ratio k_o/μ_m (hereafter termed the "Darcy coefficient") appears in the melt retention number Mr as a single parameter, the exploration of parameters leads to variations in three independent quantities in each scenario for the solid depletion, while all other parameters are taken to be fixed.

[29] Three distinct types of behavior are found for the timing of the onset of instability. For the higher range of viscosities and melt percolation rates considered, no significant circulation occurs during or after extension, and the

instability is very weak or essentially nonexistent. For the spinel stability cases, a mantle viscosity μ_0 less than 10^{20} Pa s is required for any significant instabilities to occur, while viscosities less than about $10^{19.5}$ Pa s are required for the occurrence of instabilities in either the garnet stability or mixed phase cases. For the lower range of reference viscosities (μ_0), Darcy coefficients (k_0/μ_m), and strain rates ($\dot{\varepsilon}_0$), the instability sets in almost immediately after extension and passive upwelling lead to the development of a thin partially molten layer. This kind of timing will be referred to as "synextensional instability," since the layer becomes unstable while extension is ongoing. For an intermediate range of reference viscosities, Darcy coefficients, and strain rates, on the other hand, instabilities do not develop during the time period of extension, but only begin to develop after the rate of extension slows significantly. However, this "postextensional instability" behavior is only observed in the spinel stability and mixed phase cases, and does not occur in any of the garnet stability cases. The "synextensional" versus "postextensional" instability distinction is shown in a series of time slices for two different spinel stability cases in Figure 6. Figure 7 shows time slices for two garnet stability cases: one in which no significant instability occurs and another in which synextensional instability occurs.

[30] The effect of various parameter values upon the occurrence of synextensional and postextensional behaviors is shown in Figure 8. The criterion used to make this distinction is the clear manifestation of instability in the layer prior to (synextensional) or after (postextensional) the rate of extension begins to tail off significantly (for times of about $|t - t_s| < t_s/5$). Interestingly, both the spinel stability and mixed phase cases exhibit synextensional or postextensional behavior for the same range of parameters. In all
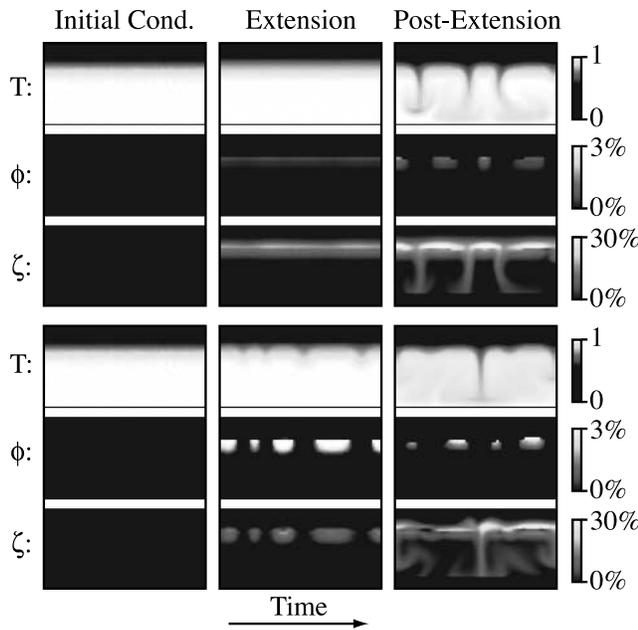
Figure 6. Plots of temperature, melt fraction, and depletion during and after extension for two spinel stability cases, showing the distinction between (top) postextensional instability and (bottom) synextensional instability.
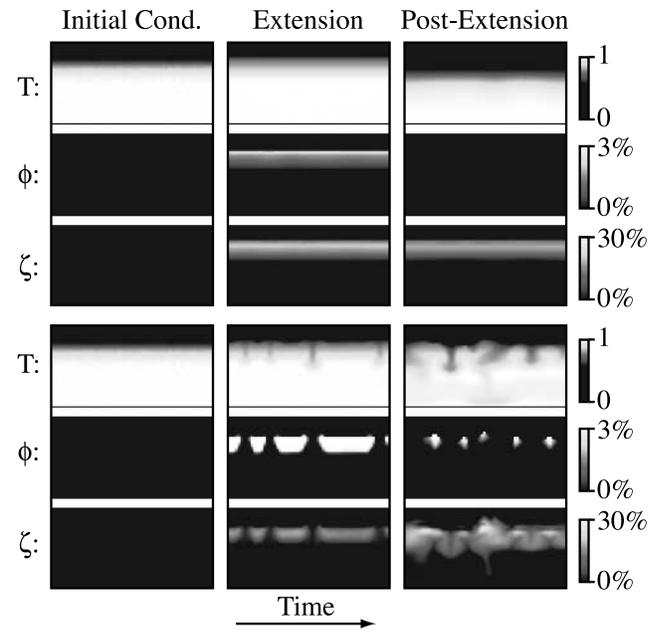
Figure 7. Plots of temperature, melt fraction, and depletion during and after extension for two garnet stability cases. (top) No significant instability. (bottom) Synextensional instability.
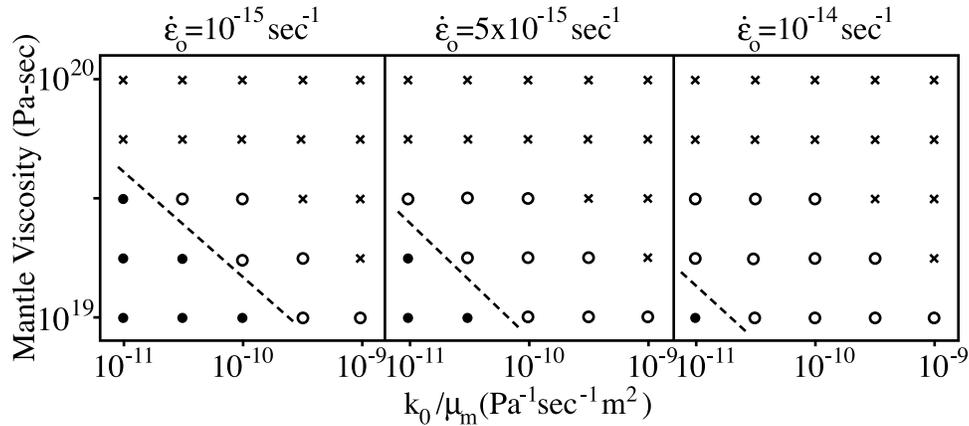
Figure 8. Dependence of synextensional (solid circles) versus postextensional (open circles) timing of instabilities upon the reference mantle viscosity μ_0 and the Darcy coefficient k_0/μ_m for three different reference strain rates $\dot{\varepsilon}_0$ in both the spinel stability and mixed phase cases and for a stretch factor of $\beta = 2$. Cases where only weak or no instabilities developed (crosses) are also indicated.

cases considered, synextensional instability is favored by a lower reference viscosity, lower rate of extension, and smaller Darcy coefficient (k_0/μ_m). The range of parameters over which the occurrence of postextensional instabilities develop becomes more narrow as the rate of extension decreases, so that for very slow extension only synextensional or weak/no instabilities should occur. For higher strain rates than those considered here, only mantle viscosities that are smaller than 10^{19} Pa s will be capable of permitting the occurrence of synextensional instabilities. A high rate of melt percolation, which rapidly drains the layer of melt, suppresses the development of instability both before and after extension in the spinel stability and mixed phase cases.

[31] A reference mantle viscosity less than 10^{20} Pa s appears to be necessary for the instabilities to develop significantly before growth of the overlying thermal boundary layer by conduction cools the partially molten layer. At much later times in the models this thermal boundary layer itself becomes unstable and "delaminates';" however, this is a fundamentally different phenomenon than the decompression melting instability. The contribution of any later thermally driven instabilities to quantities of interest is therefore removed. However, it is important to distinguish this effect from the postextensional instability behavior seen in this study when it produces melt at later times, since additional pulses of melting can also occur that could be confused with a postextensional instability. In practice, the timescales involved in the growth and subsequent "delamination" of a portion of the thermal boundary layer (on the order of several tens of millions of years) are much longer than the timescales over which the decompression melting instabilities take place (on the order of a few million years), and as a consequence the two phenomena can easily be distinguished based upon their relative timing.

[32] The synextensional versus postextensional distinction in behavior can also be seen in the time series of the total cumulative erupted volume of melt. Figures 9 and 10 show the volume of erupted melt over time for three different strain rates and for different values of the Darcy coefficient. Extension alone produces a linearly increasing volume of melt that saturates and begins to level off as extension slows. Synextensional instabilities are characterized by a growth in erupted volume of melt prior to the slowing of extension, and the total amount of erupted melt is usually larger in these cases than in postextensional cases. Postextensional instabilities, on the other hand, yield erupted volumes that initially follow extension-induced eruption rates and only after production begins to plateau does a second pulse in increased erupta begin to develop. The spinel stability cases illustrate that the propensity for synextensional instability is correlated with the total volume and rate of erupted melt, with postextensional affinity associated with a greater time lag in the onset of instability. The garnet stability cases, on the other hand, yield a much smaller variation in erupted volume with time and do not exhibit a clear signal heralding the onset of instability similar to those seen in the time series for the spinel stability cases.

[33] The cumulative total erupted volume of melt, termed the "total erupta," is plotted in Figure 11 for the same values of the strain rate. The total erupta usually increases as both k_0/μ_m and μ_0 decrease, while the spinel stability cases generated significantly more melt than either the garnet stability or mixed phase cases. In some cases, the total erupta is also smaller for the smallest values of the Darcy coefficient, a phenomenon also observed in the study of *Tackley and Stevenson* [1993] for higher values of *Mr*. The mixed phase cases exhibit a total erupta similar to that found in the garnet stability cases, but slightly smaller in volume. In either case where solid depletion buoyancy is present, the downward entrainment of the depleted material into the underlying mantle is suppressed.

4. Discussion

[34] The numerical modeling results presented above reveal a range of interesting behavior for the occurrence of the instability, its timing relative to extension, the effects of solid depletion buoyancy, and a strong influence of percolation. All of the features seen in this study carry observational consequences for the spatiotemporal charac-
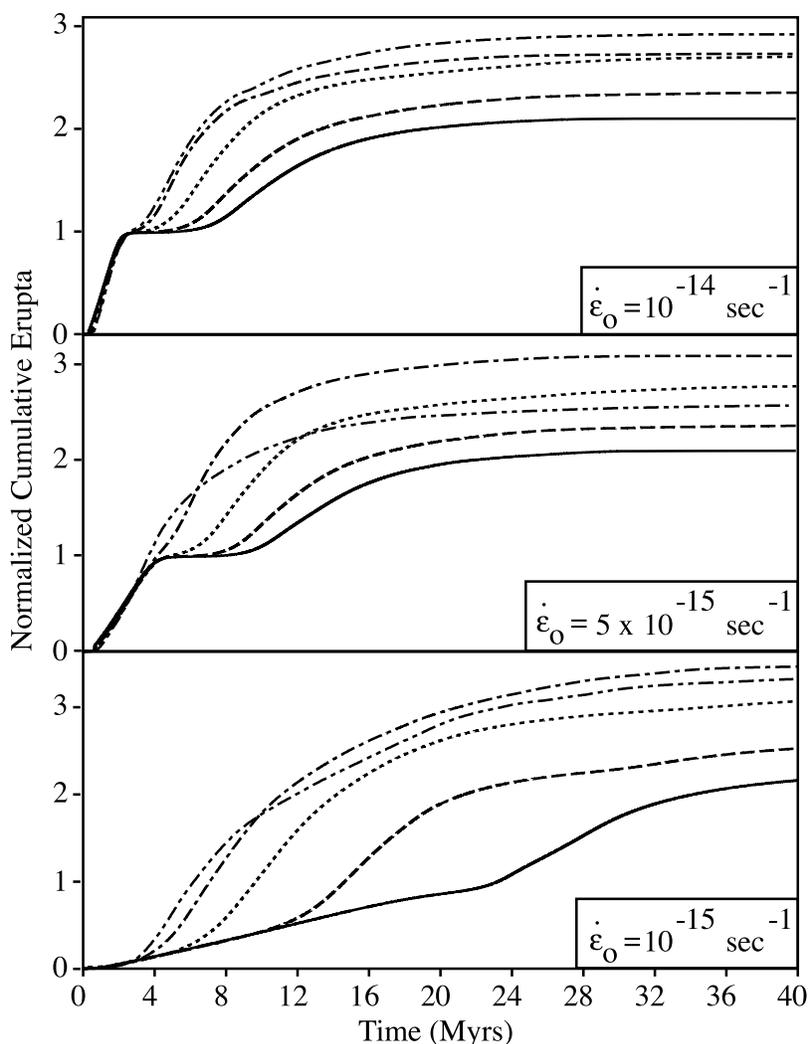
Figure 9. Time series of the cumulative erupted volume of melt in spinel stability cases with $\mu_0 = 10^{19}$ Pa s and $\beta = 2$ for three different strain rates, where the values are normalized by the volume of melt erupted by extension alone. Solid curves are cases having $k_0/\mu_m = 10^{-9}$ m^2 Pa s^{-1}, dashed curves $k_0/\mu_m = 10^{-9.5}$ m^2 Pa s^{-1}, dotted curves $k_0/\mu_m = 10^{-10}$ m^2 Pa s^{-1}, dot-dashed curves $k_0/\mu_m = 10^{-10.5}$ m^2 Pa s^{-1}, and double-dot-dashed curves $k_0/\mu_m = 10^{-11}$ m^2 Pa s^{-1}.

teristics of volcanism in regions that have undergone diffuse lithospheric extension. Here we discuss these issues in greater detail.

4.1. Synextensional Versus Postextensional Instability

[35] The lack of instabilities during extension for some of the cases suggest that the instability in this scenario is not strictly analogous to a Rayleigh-Taylor instability, since this kind of terminology carries the implication of unconditionally unstable behavior. A better analogy might be a Rayleigh-Bènard type of behavior, where some critical value or parameter must be exceeded in order for instabilities to occur. However, as the occurrence of instabilities depend upon the strain rate, it appears that any such "Rayleigh number" describing the onset of convection must itself depend upon the rate of extension. The most direct consequence of an increased extension rate is a higher rate of passive upwelling and melt production in the partially molten layer, which is accompanied by a larger fraction of retained melt. While it

seems counterintuitive that a larger amount of retained melt suppresses the onset of instability, it is shown in HST that this arises due to the presence of an increased rate of percolation in the basic state, with which the growth of any instability must compete in order to sustain lateral variations in melt fraction.

[36] The results also demonstrated that the timing of instability is highly sensitive to the depth distribution of density changes accompanying solid depletion. In particular, an absence of large density changes at depths smaller than 80 km allowed for postextensional behavior, while a uniform strong density change everywhere promoted synextensional behavior. Thus the conclusion of *Schutt and Lesher* [2006] that density changes at shallower depths are small is important in assessing whether or not postextensional instability behavior can actually occur in Earth's mantle.

[37] If instability occurs during extension, the distribution of mantle melt production will be very different than the
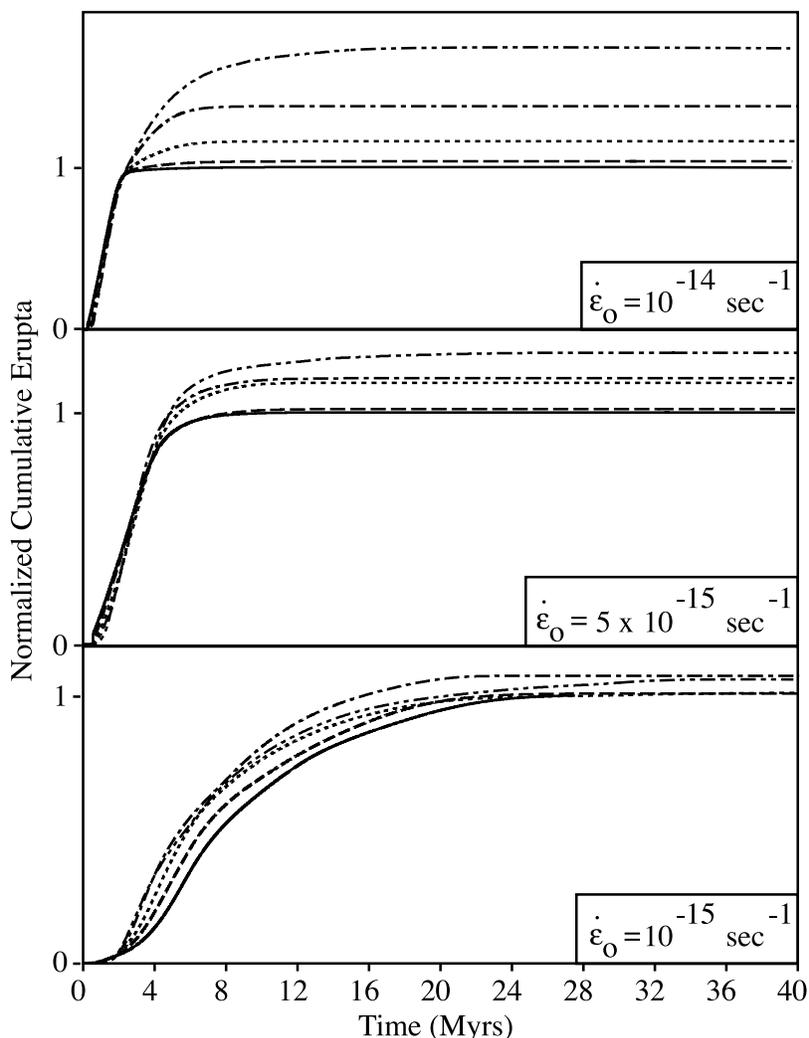
Figure 10. Time series of the cumulative erupted volume of melt in garnet stability cases with $\mu_0 = 10^{19}$ Pa s and $\beta = 2$ for three different strain rates, where the values are normalized by the volume of melt erupted by extension alone. Solid curves are cases having $k_0/\mu_m = 10^{-9}$ m^2 Pa s^{-1}, dashed curves $k_0/\mu_m = 10^{-9.5}$ m^2 Pa s^{-1}, dotted curves $k_0/\mu_m = 10^{-10}$ m^2 Pa s^{-1}, dot-dashed curves $k_0/\mu_m = 10^{-10.5}$ m^2 Pa s, and double-dot-dashed curves $k_0/\mu_m = 10^{-11}$ m^2 Pa s^{-1}.

case where instability only sets in after extension has stopped. In all cases where a significant synextensional instability was observed in the numerical models, only upwelling regions exhibited a nonzero fraction of melt while the downwellings were frozen. (The exceptions were cases where a weak or no significant instability occurred at all, resulting in no significant gain in melt production relative to extension alone.) The lack of melt in downwelling portions of the circulation reflects the fact that the flow which arose due to the instability (excluding the "no-instability" cases) was greater in magnitude than the passive upwelling velocity due to imposed extension. Thus there is a net downward motion of material in the downwelling regions even though extension has the effect of imposing a net upward motion upon the entire partially melting layer.

[38] Because melt is produced only in upwelling portions of an unstable partially melting layer, magma delivered to the crust by this mechanism will tend to be localized above regions that are correlated with upwelling asthenospheric

flow arising from the instability. The consequences for the spatial distribution of magmatism (and possibly volcanism if melt reaches the surface) in the crust is shown schematically in Figure 12. The cumulative melt production for postextensional instabilities will be characterized by the development of a distribution of magmatism consistent with extension alone (which is uniform in the cases considered here), followed by localized delivery of melt above upwelling portions of the instability. Synextensional instability, on the other hand, will exhibit very little magmatism in areas overlying downwelling currents, so that the majority of melt production will be focused in patches above upwellings. Thus the different distributions of magmatism (or possibly volcanism) in the crust predicted for synextensional versus postextensional instabilities may present a good diagnostic for the characteristics of any asthenospheric instabilities occurring beneath extensional provinces. However, this is not necessarily a unique diagnostic. A potential complication is the uncertainty of the initial condition in any part of
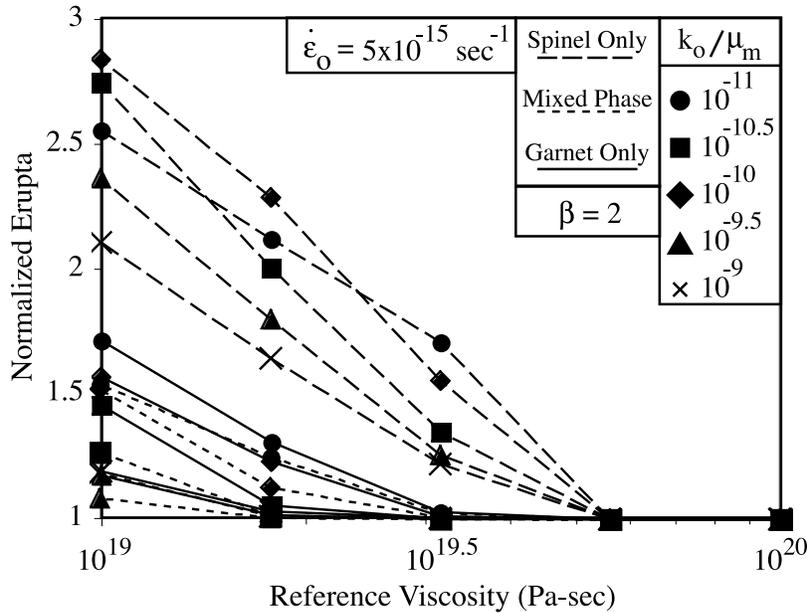
Figure 11. Total erupted volume of melt normalized by the volume of melt erupted by extension alone for a strain rate of $\dot{\varepsilon}_0 = 5 \times 10^{-15}$ s^{-1}. Each series is labeled by its value of k_0/μ_m, which is given in units of m^2 Pa s^{-1}.

the upper mantle prior to extension. For example, some regions of the upper mantle could be cooler or more highly depleted relative to adjacent material prior to extension, so that a decreased propensity for melt production already exists in some locations at the outset. It is important to note that this sort of preexisting lateral heterogeneity will also influence the behavior of the instability because only some portions of the upwelling asthenosphere are capable of producing melt. Such an arrangement would be expected to influence the pattern of any upwelling and downwelling flow, and might promote the occurrence of synextensional instabilities.

4.2. Melt Buoyancy and Production

[39] The cumulative "erupted" volume of melt was found to be sensitive to both the viscosity μ_0 and Darcy coefficient k_0/μ_m in all cases where a significant instability developed. The simultaneous balance between melt percolation, production, and buoyant circulation is central to understanding how these physical parameters affect the total volume of melt. A simple model may be constructed to show how the combination of these factors gives rise to the strong influence of μ_0 and k_0/μ_m upon the total erupta observed in the numerical models.

[40] First, consider upwelling in a layer at the eutectic with bulk nondimensional velocity v_c' (primes will again be used to denote nondimensionalized quantities in this section). Here, v_c' will refer to the magnitude of the buoyant circulation rather than the rate of passive upwelling. A simple balance between melt production and percolation (ignoring the effects of compaction and advection) yields an approximate characteristic melt fraction

$$\phi_c \approx \sqrt{\frac{MrF'v_c'}{Rm}}, \qquad (26)$$

where the dimensional length scale D is taken to be the thickness of the partially molten layer. Here, ϕ_c is intended to be only a representative value of ϕ rather than a full solution. The more general case is presented in HST [see also *Schmeling*, 2000].

[41] Now consider a stationary bulk circulation within a partially molten layer with an aspect ratio of unity. In this case the vertical velocity field can be roughly approximated by $v_z' = v_c' \sin(\pi x) \sin(\pi z)$, where v_c' is now identified with the characteristic amplitude of the circulation. The flow is driven by a "rectified" buoyancy force arising from partial melt that can be crudely approximated as $Rm\phi_c \sin(\pi x) \sin(\pi z)/2$, where the factor of 2 is included to account for the lack of melt in downwellings. A simple momentum balance in the absence of thermal or depletion buoyancy forces then gives

$$v_c' \approx \frac{Rm\phi_c}{8\pi^2}. \qquad (27)$$

This is the characteristic diapiric rise rate for upwelling of rock containing a fraction of melt ϕ_c.

[42] Combining equations (26) and (27) yields an approximate value for the fraction of melt supported by buoyant circulation:

$$\phi_c \approx \frac{MrF'}{8\pi^2}; \qquad (28)$$

ϕ_c does not depend upon Rm because melt buoyancy drives bulk circulation (and hence production) as well as percolation of melt out of the layer, with the net result that the two effects cancel one another. Another expression for
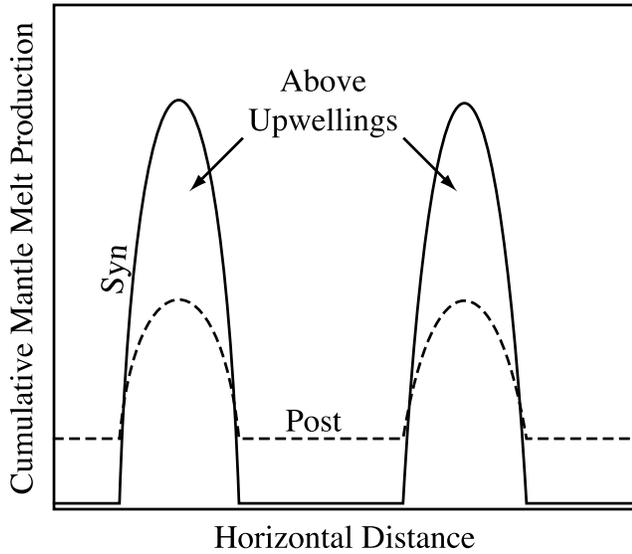
Figure 12. Schematic illustration of the differing distributions of mantle melt production depending upon whether synextensional (solid line) or postextensional (dashed line) instabilities occur. The flat background distribution in both cases is due to extension in the absence of instabilities, while the peaks are correlated with locations lying above upwellings portions of the circulation resulting from instability. A synextensional instability occurs early during extension, suppressing the production of melt in locations above downwelling portions of the resulting circulation, while a postextensional instability allows extension to produce a greater amount of melt prior to forming localized patches of magma production.

the velocity amplitude can be obtained that only depends on the parameters Rm, Mr, and F',

$$v_c' \approx \frac{RmMrF'}{64\pi^4}. \tag{29}$$

The proportionalities expressed by equations (28) and (29) are in good agreement with the modeling results of *Tackley and Stevenson* [1993], which only considered partial melt buoyancy as a driving force for the instability.

[43] In terms of the dimensional velocity ($v_c = v_c'\kappa/D$), equation (29) leads to the proportionality

$$v_c \propto \frac{\Delta\rho_M g F D^5}{\mu_o^2(k_0/\mu_m)}, \tag{30}$$

where $\Delta\rho_M = \rho_s - \rho_m$. The dimensional velocity is seen to scale inversely to the square of the viscosity. This nonlinear behavior can be understood by noting that the strength of the buoyancy source ($\propto Rm\phi_c$) itself depends on the circulation rate v_c, with higher rates supporting a proportionally greater fraction of melt in upwellings, and consequently receiving the benefit of extra buoyancy. Estimates for the importance of melt buoyancy in this kind of system must therefore take into account the fact that the retained fraction of melt is itself proportional to the circulation.

[44] This nonlinear behavior for the role of melt buoyancy can help explain the strong sensitivity of erupted melt upon viscosity and the Darcy coefficient. For example, the rate of melt production due to buoyant circulation in the layer, $\dot{Q}$, is necessarily proportional to $v_c F$, so that,

$$\dot{Q} \propto \frac{\Delta\rho_M g F^2 D^5}{\mu_o^2(k_0/\mu_m)}. \tag{31}$$

Defining an effective duration of the circulation τ_c (which need not be constant for all parameter values) such that the column height of melt H erupted at the surface is $H = \dot{Q}\tau_c D$:

$$H \propto \frac{\Delta\rho_M g \tau_c F^2 D^6}{\mu_o^2(k_0/\mu_m)}. \tag{32}$$

The proportionality relation in (32) captures the observed dependence of erupted melt upon k_0/μ_m as well as the strong dependence upon the reference viscosity. It is worth noting that this kind of dependence would not be present if the value of ϕ_c were imposed as a constant, since it would no longer be coupled to the characteristic velocity of the circulation. It is also apparent that the dependence of H upon F is not linear, and therefore caution should be taken in extrapolating any results presented in this study to different values of F.

4.3. Effects of a Buoyant Depleted Layer

[45] Unlike partial melt, depletion is a cumulative property that generally increases with the degree of upward displacement (instead of upward velocity) of material in the partially molten layer. Therefore the effects of buoyant melt depletion of the solid residuum are inherently different than the type of behavior described above for melt buoyancy. In the garnet stability cases, a buoyant depleted layer formed as a consequence of passive upwelling following extension, and the volume of melt produced by the instability was generally less than in the spinel stability cases. However, the cumulative amount of erupted melt still depends upon k_0/μ_m even in these cases. This behavior makes sense if one considers that lower values of viscosity and rates of melt percolation can nevertheless enhance the ability for melt buoyancy to push depleted material aside and for downwellings to entrain some of this material downward, as described by *Jha et al.* [1994].

[46] This resistance to downward entrainment of the depleted layer in the mixed phase and garnet stability cases is a likely explanation for the reduced total volumes of erupted melt measured in these scenarios because it opposes the tendency for deeper (and longer duration) circulation. It is somewhat surprising that the garnet stability cases produced slightly more erupta than the mixed phase cases, since the latter scenario is intermediate between the end-member garnet and spinel stability cases. The reason for the slight gain in melt productivity in the garnet stability cases relative to the mixed phase cases might be attributable to the fact that the former always exhibited synextensional behavior, while the latter exhibited postextensional instability for certain ranges of parameters.
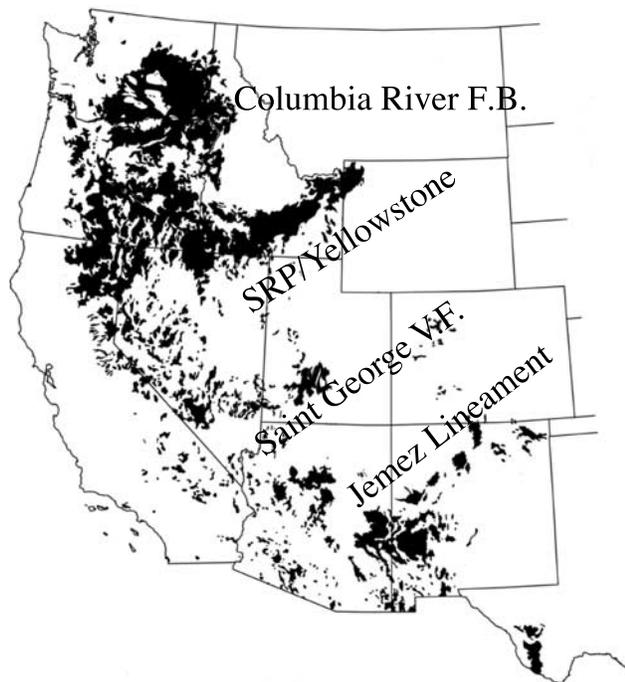
Figure 13. Map showing the occurrence of Miocene and younger volcanic rocks in the western United States, with the locations of the Columbia River Flood Basalts, Snake River Plain (SRP)/Yellowstone trend, Jemez Lineament, and St. George volcanic field indicated.

4.4. Western United States Basin and Range Volcanism

[47] The suppression of buoyant decompression melting instabilities by extension is a surprising characteristic of this type of instability. This kind of behavior can lead to distinctive observational consequences if these instabilities occur in regions undergoing lithospheric extension because there is no other straightforward dynamical process which would produce a similar spatiotemporal pattern of volcanism without appealing to ad hoc mechanisms. While there are many extensional provinces on Earth, none offers better geological exposure and geophysical coverage than the Basin and Range province of the western United States. In this region, the relationship between volcanism and extension have long been a subject of debate, and the results found in this study might offer some insights into the nature of recent volcanic activity in this province.

[48] During the late Cenozoic (mid-Miocene), much of the western United States underwent large-scale diffuse lithospheric extension, with elongation of the crust mostly accommodated by a fault-block mode of deformation that is largely responsible for the present-day "horst and graben" physiography of the Basin and Range province. This "Basin and Range" episode of extension followed earlier episodes of localized high-magnitude extension which is characterized by unroofing of the upper crust along detachment faults [e.g., *Axen et al.*, 1993]. Thermochronological constraints in the Great Basin region indicate that the duration of mid-Miocene extension was relatively short (on the order of a million years) and largely contemporaneous [*Stockli et al.*, 2002]. The Cenozoic volcanic history of this region is also temporally bimodal, with ubiquitous episodes of ignimbrite

volcanism in the mid to late Tertiary followed by increasingly basaltic volcanism from the mid-Miocene to present [e.g., *Christiansen and Lipman*, 1972].

[49] The simplest model for the origin of volcanism accompanying lithospheric extension is passive upwelling and attendant decompression melting of the underlying mantle [e.g., *McKenzie and Bickle*, 1988]. Because magma produced in the mantle travels upward into the crust relatively rapidly, this basic hypothesis predicts that the amount and rate of volcanism should be well correlated (both in space and time) with extension. However, these predictions are not borne out by observations in much of the western U.S. Basin and Range province. In particular, much of the Miocene to present basaltic volcanism tends to be focused in several areas (see Figure 13), even though the Basin and Range episode of extension is more uniformly distributed. Additionally, the temporal relationship between volcanism and extension in the Basin and Range province is not straightforward [e.g., *Axen et al.*, 1993], and in many locations an anticorrelation between rates of extension and volcanism have been reported [*Gans and Bohrson*, 1998; *Stockli et al.*, 2002]. While the silicic volcanic activity commonly preceding extension in this region is often attributed to delamination and foundering of the shallowly subducted Farallon plate [e.g., *Humphreys*, 1995], there is no straightforward mantle process which could explain both the localization and increase in volcanic activity after the cessation of extension. One possible exception is the fortuitous arrival of several mantle plumes from the deep mantle. However, a mantle plume origin of volcanism in the western United States (with the exception of the Columbia River flood basalts and Snake River Plain/Yellowstone system) is probably not tenable because the characteristic time progression in ages of volcanic centers expected of this mechanism is not observed. The temporal anticorrelation between extension and volcanism is pronounced in the regions surrounding the Colorado plateau, such as the St. George volcanic field and Jemez Lineament [*Gans and Bohrson*, 1998].

[50] The strong suppression of volcanism during extension remains a rather surprising observation. This apparent dilemma is exacerbated by the fact that magma transport through crustal dikes and cracks should be enhanced while the crust is undergoing extension [e.g., *Rubin*, 1995]. *Gans and Bohrson* [1998] proposed that a loss of confining pressure in the middle crust attending extension might lead to devolatilization and subsequent freezing of midcrustal magmas, an effect that might be enhanced by the onset of hydrothermal convection in the upper crust which would transport heat more rapidly toward the surface. This type of effect was proposed as a mechanism to impede transmission of magma to the surface. While reduced rates of magma transmission through the crust during extension may or may not explain the relative suppression of volcanism during extension, these mechanisms alone cannot explain an increase in the rate of volcanism following extension, which requires a renewed source of mantle melting that cannot be generated by simple passive decompression melting.

[51] The occurrence of anomalously low seismic velocity anomalies at asthenospheric depths ($\sim$60–100 km) beneath several Miocene and younger volcanic centers in the western United States led *Humphreys and Dueker* [1994b] to posit the

existence of asthenospheric instabilities in the form of small-scale convection rolls, with the axes of upwelling coinciding with linear trends of volcanism in the Jemez lineament (New Mexico and Arizona), St. George volcanic field (southern Utah), and possibly the Snake River Plain/Yellowstone system. They hypothesized that these rolls formed under the influence of mantle shear accompanying the southwestward motion of the North American plate, and were significantly influenced by density variations arising from partial melt and depletion of the solid residuum. Changes in deep-rooted lithospheric structure along these trends (e.g., the edges of the Colorado plateau) might also explain the spatial distribution of these fields. Such a mechanism could explain the spatial distribution of some Basin and Range volcanism and a variety of geophysical observations [*Humphreys and Dueker*, 1994b].

[52] The instability behavior offers a potentially useful way to explain renewed localized volcanism following Basin and Range extension. The observable effects of the timing and rate of magma production in the mantle asthenosphere will, of course, be strongly affected by any suppression of magma transport through the crust. Thus it is not straightforward to directly map rates of eruption measured in the present numerical models into expected rates of volcanism at the surface for comparison to real data. The timescales and volumes of melt generated by instabilities seen in the present study and in previous studies [*Tackley and Stevenson*, 1993; *Raddick et al.*, 2002] can easily satisfy a wide range of measured durations in postextensional volcanism in the western United States (typically of order several million years). Rates of extension inferred in several volcanic fields of the Basin and Range province [e.g., *Gans and Bohrson*, 1998; *Stockli et al.*, 2002] may be somewhat higher than those considered in the numerical models presented in this study (by up to a factor of about two), enhancing the possibility for postextensional behavior. On the other hand, petrological constraints indicate that melting beneath the southern portion of the Great Basin occurred at depths extending into the garnet peridotite stability field [e.g., *Wang et al.*, 2002], and therefore solid depletion density changes at shallower depths remains an important issue.

5. Summary and Conclusion

[53] Buoyant decompression melting instabilities beneath extending lithosphere can have a significant effect upon the generation of melt in the underlying mantle and the spatiotemporal characteristics of any consequent magmatism and/or volcanism. These instabilities produce more melt than extension alone but require a sufficiently small asthenospheric viscosity (i.e., less than 10^{20} Pa s) and gains in melt production are strongly suppressed by solid depletion buoyancy. Suppression of unstable behavior during extension is another potentially important phenomenon that depends upon the depth distribution of density changes accompanying melt depletion as well as the rate of extension. In a companion paper, this behavior is assessed in greater detail using a linear stability analysis.

[54] The results of this study also illustrate the importance of the background processes leading to the formation of a partially molten layer. Several previous studies of the buoyant decompression melting instability have often begun with an idealized initial condition in which the process of bringing about a partially molten layer has been ignored, and a thick portion of mantle already finds itself at the solidus. The results of this study demonstrate that the process by which a layer of mantle is brought to the solidus can have dramatic effects upon the characteristics of the instability, and therefore cannot be neglected. This is due in part to the important influence of melt percolation and the cumulative degree of depletion the layer obtains upon bringing it to a partially molten state.

[55] The explicit treatment of melt percolation also appears to be critical in assessing the physics and observational consequences of this kind of instability. If a threshold value is used instead where melt is instantly erupted at some critical fraction, the ability for melt buoyancy to grow nonlinearly with the rate of circulation will be suppressed once it reaches saturation. As a result, many of the features of the instability observed in this study would be entirely absent. This finding is amplified by the results of the linear stability analysis in the companion paper.

References

Anderson, D. L., and C. G. Sammis (1970), Partial melting in the upper mantle, *Phys. Earth Planet. Inter.*, *3*, 41–50.

Asimow, P. D., M. M. Hirschmann, and E. M. Stolper (1997), An analysis of variations in isentropic melt productivity, *Philos. Trans. R. Soc. London*, *355*, 255–281.

Axen, G. J., W. J. Taylor, and J. M. Bartley (1993), Space-time patterns of the onset of extension and magmatism, southern Great Basin, Nevada, Utah, and California, *Geol. Soc. Am. Bull.*, *105*, 56–76.

Barnouin-Jha, K., E. M. Parmentier, and D. W. Sparks (1997), Buoyant mantle upwelling and crustal production at oceanic spreading centers: On-axis segmentation and off-axis melting, *J. Geophys. Res.*, *102*, 11,979–11,990.

Bercovici, D., Y. Ricard, and G. Schubert (2001), A two-phase model for compaction and damage: 1. General theory, *J. Geophys. Res.*, *106*, 8887–8906.

Buck, W. R., and W. S. Su (1993), Buoyancy effects on mantle flow under mid-ocean ridges, *J. Geophys. Res.*, *98*, 12,191–12,205.

Choblet, G., and E. M. Parmentier (2001), Mantle upwelling and melting beneath slow spreading centers: Effects of variable rheology and melt productivity, *Earth Planet. Sci. Lett.*, *184*, 589–604, doi:10.1016/S0012-821X(00)00330-7.

Christiansen, R. L., and P. W. Lipman (1972), Cenozoic volcanism and plate-tectonic evolution of the western United States. II. Late Cenozoic, *Philos. Trans. R. Soc. London, Ser. A*, *271*, 249–284.

Crane, K. (1985), The spacing of rift axis highs: Dependence upon diapiric processes in the underlying asthenosphere, *Earth Planet. Sci. Lett.*, *72*, 405–414.

Gans, P. B., and W. A. Bohrson (1998), Suppression of volcanism during rapid extension in the Basin and Range province, United States, *Science*, *279*, 66–68.

Hernlund, J. W., D. J. Stevenson, and P. J. Tackley (2008), Buoyant melting instabilities beneath extending lithosphere: 2. Linear analysis, *J. Geophys. Res.*, doi:10.1029/2006JB004863, in press.

Humphreys, E. D. (1995), Post-Laramide removal of the Farallon slab, western United States, *Geology*, *23*, 987–990.

Humphreys, E. D., and K. G. Dueker (1994a), Western U.S. upper mantle structure, *J. Geophys. Res.*, *99*, 9615–9634.

Humphreys, E. D., and K. G. Dueker (1994b), Physical state of the western U.S. upper mantle, *J. Geophys. Res.*, *99*, 9635–9650.

Jha, K., E. M. Parmentier, and J. P. Morgan (1994), The role of mantle-depletion and melt-retention buoyancy in spreading-center segmentation, *Earth Planet. Sci. Lett.*, *125*, 221–234.

Jordan, T. H. (1979), Mineralogies, densities and seismic velocities of garnet lherzolites and their geophysical implications, in *The Mantle Sample: Inclusions in Kimberlites and Other Volcanics, Proceedings of the Second International Kimberlite Conference*, vol. 2, edited by F. R. Boyd and H. O. A. Meyer, pp. 1–14, AGU, Washington, D. C.

Lingenfelter, R. E., and G. Schubert (1974), Hot spot and trench volcano separations, *Nature*, *249*, 820.

McKenzie, D. (1984), The generation and compaction of partially molten rock, *J. Petrol.*, *25*, 713–765.

McKenzie, D., and M. J. Bickle (1988), The volume and composition of melt generated by extension of the lithosphere, *J. Petrol.*, *29*, 625–679.

Oxburgh, E. R., and E. M. Parmentier (1977), Compositional and density stratification in the oceanic lithospherecauses and consequences, *J. Geol. Soc. London*, *133*, 343–354.

Parmentier, E. M., and J. P. Morgan (1990), Spreading rate dependence of three-dimensional structure in oceanic spreading centres, *Nature*, *348*, 325–328.

Raddick, M. J., E. M. Parmentier, and D. S. Scheirer (2002), Buoyant decompression melting: A possible mechanism for intraplate volcanism, *J. Geophys. Res.*, *107*(B10), 2228, doi:10.1029/2001JB000617.

Ribe, N. M., and U. R. Christensen (1999), The dynamical origin of Hawaiian volcanism, *Earth Planet. Sci. Lett.*, *171*, 517–531.

Ricard, Y., D. Bercovici, and G. Schubert (2001), A two-phase model for compaction and damage: 2. Applications to compaction, deformation, and the role of interfacial surface tension, *J. Geophys. Res.*, *106*, 8907–8924.

Rubin, A. M. (1995), Propagation of magma-filled cracks, *Annu. Rev. Earth Planet. Sci.*, *23*, 287–336.

Schmeling, H. (2000), Partial melting and melt segregation in a convecting mantle, in *Physics and Chemistry of Partially Molten Rocks*, edited by N. Bagdassarov, D. Laporte, and A. B. Thompson, pp. 141–178, Kluwer Acad., Norwell, Mass.

Schruben, P. G., R. E. Arndt, and W. J. Bawiec (1998), Geology of the conterminous United States at 1:2,500,000 scale—A digital representation of the 1974 P. B. King and H. M. Beikman map, *USGS Digital Data Ser.11*, Release 2, U.S. Geol. Surv., Reston, Va. (Available at http://pubs.usgs.gov/dds/dds11/)

Schutt, D. L., and C. E. Lesher (2006), Effects of melt depletion on the density and seismic velocity of garnet and spinel lherzolite, *J. Geophys. Res.*, *111*, B05401, doi:10.1029/2003JB002950.

Scott, D. R., and D. J. Stevenson (1989), A self-consistent model of melting, magma migration and buoyancy-driven circulation beneath mid-ocean ridges, *J. Geophys. Res.*, *94*, 2973–2988.

Spiegelman, M. (1993), Flow in deformable porous media, part 1, simple analysis, *J. Fluid Mech.*, *247*, 17–38.

Stevenson, D. J. (1988), Rayleigh-Taylor instabilities in partially molten rock, *Eos Trans. AGU*, *69*, 1404.

Stockli, D. F., B. E. Surpless, T. A. Dumitru, and K. A. Farley (2002), Thermochronological constraints on the timing and magnitude of Miocene and Pliocene extension in the central Wassuk Range, western Nevada, *Tectonics*, *21*(4), 1028, doi:10.1029/2001TC001295.

Stolper, E., and D. Walker (1980), Melt density and the average composition of basalt, *Contrib. Mineral. Petrol.*, *74*, 7–12.

Tackley, P. J. (1996), Effects of strongly variable viscosity on three-dimensional compressible convection in planetary mantles, *J. Geophys. Res.*, *101*, 3311–3332.

Tackley, P. J., and D. J. Stevenson (1993), A mechanism for spontaneous self-perpetuating volcanism on the terrestrial planets, in *Flow and Creep in the Solar System: Observations, Modeling, and Theory*, edited by D. B. Stone and S. K. Runcorn, pp. 307–322, Kluwer Acad., Norwell, Mass.

Turcotte, D. L., and G. Schubert (2002), *Geodynamics*, 2nd ed., Cambridge Univ. Press, New York.

Wang, K., T. Plank, J. D. Walker, and E. I. Smith (2002), A mantle melting profile across the Basin and Range, SW United States, *J. Geophys. Res.*, *107*(B1), 2017, doi:10.1029/2001JB000209.

Whitehead, J. A., H. J. B. Dick, and H. Schouten (1984), A mechanism for magmatic accretion under spreading centres, *Nature*, *312*, 146–148.

————————

J. W. Hernlund, Department of Earth and Ocean Sciences, University of British Columbia, 6339 Stores Road, Vancouver, BC, Canada V6T 1Z4. (hernlund@gmail.com)

D. J. Stevenson, Division of Geological and Planetary Sciences, California Institute of Technology, 1200 E. California Blvd., Pasadena, CA 91125, USA.

P. J. Tackley, Institute for Geophysics, ETH-Zurich, Hönggerberg HPP L13, Schafmattstrasse 30, CH-8093 Zurich, Switzerland.